

# Enhancement of Angular Resolution of a Flat-Base Luneburg Lens Antenna by Using Correlation Method

Xiang Gu<sup>1, 2, \*</sup>, Sidharath Jain<sup>3</sup>, Raj Mittra<sup>1</sup>, and Yunhua Zhang<sup>2</sup>

**Abstract**—We propose a technique for enhancing the angular resolution of a flat-base Luneburg lens antenna to enable it to detect multiple targets with arbitrary scattering cross-sections that are located in angular proximity. The technique involves measuring the electric field distribution on the flat plane of the Luneburg lens antenna, operating in the receive mode, at a specified number of positions, and correlating these distributions with the known distributions derived from the field distributions in the measurement plane generated by single target at different look angles. We show that the proposed approach can achieve enhanced resolution than the basis of the beam-width of the Luneburg lens antenna, and it is capable of distinguishing between two targets with different scattering cross-sections that have an angular separation as small as  $1^\circ$  for a Luneburg lens with  $6.35\lambda$  aperture size, for Signal-to-Noise Ratio (SNR) better than 20 dB.

## 1. INTRODUCTION

Wide-angle scanning and high angular resolution are often concerned and desired in many modern radar applications, e.g., wireless communication, air navigation, automotive radar, etc., and mechanically steerable antennas and phased arrays are traditionally used for such applications [1]. However, such antennas are usually operated by a mechanical rotation device that cannot meet the requirements of rapid beam-scanning and flexible control. On the other hand, the phased arrays are more sophisticated and can serve multiple functions for different applications. However, they can be bulky, expensive to fabricate and often require signal processing hardware.

There has been considerable interest in the design of antennas capable of significantly increasing the directivity, lowering the sidelobe levels, increasing the angular scanning range, by combining the features of lenses [2, 3]. The lens proposed by Luneburg [4], which has the capability of all-angle-scan regardless of the frequency of operation, as well as excellent focusing characteristics, is an attractive candidate for many applications such as multi-beam antennas, multi-frequency scanning, and spatial scanning. The characteristics of the Luneburg lens have been studied in many papers [5, 6]. They show that the Luneburg lens has superior performance compared with conventional lenses made of uniform materials because it can perfectly focus the incoming electromagnetic waves on its opposite spherical surface. However, its spherically symmetric gradient-index dielectric configuration is not only incompatible with the planar feeding and receiving devices, but it also poses some difficulties in fabrication. In the past few years, many researches have focused on the manufacture and realization of the Luneburg lens, as well as its applications, which include the design and implementation of a 2D and 3D Luneburg lens antenna by using printed circuit board [7], an array of size-varying circular patches on a dielectric substrate inside a Parallel-Plate Waveguide (PPW) structure [8], a Sievenpiper “mushroom” array [9], loaded wire

---

*Received 18 June 2014, Accepted 4 August 2014, Scheduled 12 August 2014*

\* Corresponding author: Xiang Gu (guxiang@mirslab.cn).

<sup>1</sup> The Electromagnetic Communication Laboratory, Department of Electrical Engineering, Pennsylvania State University, University Park, PA 16802, USA. <sup>2</sup> The Key Laboratory of Microwave Remote Sensing, Center for Space Science and Applied Research, Chinese Academy of Sciences, Beijing 100190, China. <sup>3</sup> Microsoft, One Microsoft Way, Redmond, WA 98052, USA.

grids [10], quasi-continuous slices [11], a liquid medium approach and a 3D-printing process [12, 13], non-resonant metamaterials [14], embedding a Vivaldi antenna source inside a parallel-plate waveguide [15], air-filled parallel plates [16], and 3D inhomogeneous and nearly isotropic gradient-index materials [17]. There are also many papers which concentrate on the applications of the Luneburg lens. In [18], an array of Luneburg lens antennas have been proposed for the Square Kilometer Array (SKA) radio telescope because of its multiple advantages of optical beam forming, inherent wide bandwidth, and very wide field of view.

In addition, Liang et al. [19] have reported an approach for Direction-Of-Arrival (DOA) estimation by using five conformal detectors located on the curved surface of a single Luneburg lens antenna to receive the signal from  $-20^\circ$  to  $20^\circ$ , the operating frequency is 5.6 GHz, and the initial direction finding results using a correlation algorithm show that the estimated error is smaller than  $2^\circ$  within  $-15^\circ$  to  $15^\circ$  incident angles. However, the range of incident angle is still limited, and the number of detectors is not enough. Recently, the present authors have proposed the design of a flat-base Luneburg lens antenna, and have investigated its scan performance and compared its performance with conventional lenses [20]. In this paper, we propose the use of such a flat-base Luneburg lens antenna for DOA estimation by using Correlation Method (CM) [21] applied to the field distribution in the receive aperture, which can not only achieve both wide-angle scanning and high angular resolution, but can also operate over a broad frequency range, as well as for different polarizations. Although we focus on the two-target case in this paper, the proposed technique can be applied in a general scenario when multiple targets are present.

## 2. DESIGN OF FLAT-BASE LUNEBURG LENS ANTENNA

The Luneburg lens is designed to focus a plane wave, arriving from an arbitrary direction, at a point which is located diametrically opposite to that of the incident side. Luneburg has shown that the problem of finding  $\varepsilon_r$  of the lens can be formulated in terms of an integral equation [4], whose solution provides us the required material parameters of the lens. They are given by:

$$\varepsilon_r = 2 - (r/R)^2 \quad (1)$$

where  $r$  is the distance from the center of the lens, and  $R$  is its radius. It is evident that if we place a feed whose phase center is located on the surface of the lens, it would transform the spherical front wave, emanating from its phase center, into a planar one. Obviously, if one wishes to scan the beam, one would have to rotate the feed around the surface of the lens, which is not the most convenient thing to do; instead, it would be considerably more desirable to place the feed array on a flat surface. With this in mind, we have proposed a design, shown in Figure 1, of a lens with a spherical profile, which preserves the salutary features of the conventional Luneburg lens but is much more convenient to feed in the transmit mode since it has a flat-base design. More details about the design can be found in [20] and are omitted here.

As shown in Figure 1, the Luneburg lens consists of 11 layers and has a diameter of 63.5 mm. The first ten layers from the center have a thickness of 3 mm each and the last layer is 1.75 mm thick. The dielectric parameters of the layers vary depending on their distance from the center, in accordance with (1). The feed is a  $6 \times 6$  waveguide array with Perfect Electric Conductor (PEC) walls that are 1 mm thick. The waveguide has a square cross-section with a side length of 9 mm. This paper focuses on the receive mode; therefore, we set an array of observers in the measurement plane, i.e., the truncation plane of the waveguides.

Figure 2 shows three possible distributions of targets which radar may be required to detect. In case 1, the two targets obviously have different time delays and they can be distinguished in time domain. In case 2, the two targets have an angular separation that is greater than the half-power beam-width; it is possible to detect them by using conventional techniques. However, in case 3, the angular separation is less than the half-power beam-width, a traditional antenna would only see a single target, located somewhere in-between the two targets. In this paper, we concentrate on the third case, which is the most difficult case in practice.

It is well known that the angular resolution of an antenna is determined by its half-power beam-width, which is inversely proportional to the aperture size of the antenna. In this paper, we calculate the half-power beam-width of the Luneburg lens as  $\lambda/D$  by assuming the aperture efficiency is unity,

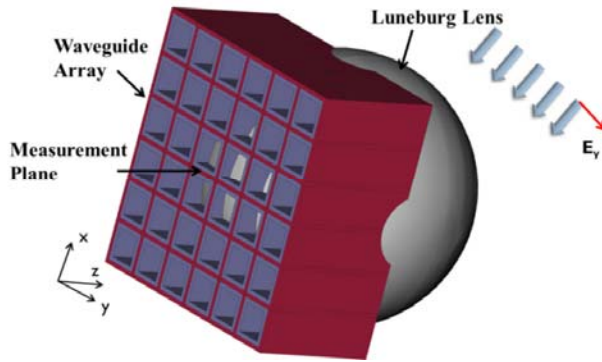


Figure 1. lat-base Luneburg lens antenna.

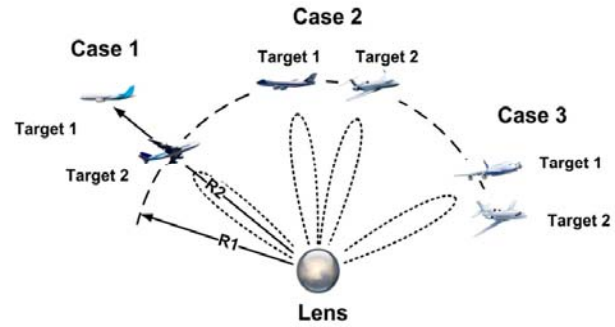


Figure 2. Multiple targets scenarios.

where  $\lambda$  is the free space wavelength and  $D$  is the diameter of the Luneburg lens. This is slightly larger than  $9^\circ$  for a diameter of  $D = 63.5$  mm at 30 GHz. Therefore, the limit of angular resolution for this antenna is nearly  $9^\circ$  by utilizing conventional techniques to process the received signal in the measurement plane by tracking the location of the maximum position.

For the case of single target located within the scan range of the lens, the field distribution in the measurement plane would be unique for each angle. Of course, the distribution would be corrupted by noise which would distort the resolution. For the case of multiple targets with unknown Radar Cross-Section (RCS) levels, the field distribution in the measurement plane is a vector sum of the field distributions generated by each target. To handle this case, we firstly create a database by superimposing the contributions with steps for the amplitude scales and phase differences, which is a valid assumption in most practical scenarios. As one might expect, the smaller the steps for the amplitude scale and the phase difference, the better is the resolution one can obtain, at the cost of increasing the time for processing.

To enhance the resolution of the above Luneburg lens, we propose to employ the correlation method, which is widely used in the areas of image and signal processing. In the following section we describe the case based on correlation method to detect multiple targets with different incident angles and different RCS levels. The scattered field from a target received by the lens can be considered to be a plane wave with initial amplitude and phase, which depends on several factors such as scattering cross-section, the distance from the target to the lens, the properties of the atmosphere, etc.. We develop the measurement database, comprising of the electric fields in the measurement plane that is induced by single and multiple targets that have different combinations of orientations, distances and scattering cross-sections. Thus, the measurement database is derived by doing a vector addition of the field distributions due to the individual targets located at different angles.

The CM is based on correlating the measured field distribution in the measurement plane due to an unknown distribution of targets with all the entries in the measurement database. The correlation coefficient ( $\rho_n$ ) for the  $n$ th entry in the database is defined as:

$$\rho_n = \frac{1}{(M_i M_j - 1) \sigma^M \sigma_n^D} \sum_{i=1}^{M_i} \sum_{j=1}^{M_j} \left[ (E^M(x_i, y_j) - \mu^M) (E_n^D(x_i, y_j) - \mu_n^D)^* \right] \quad (2)$$

where the superscript ‘ $M$ ’ denotes the field distribution in the measurement plane induced by the targets; the superscript ‘ $D$ ’ denotes the known field distribution in the measurement plane, which is stored in the database; and  $\mu$  and  $\sigma$  refer to the mean and standard deviation of the field distribution, respectively.  $M_i$  and  $M_j$  are the number of sample points in the measurement plane along  $x$ - and  $y$ -directions, respectively. The value of  $n$  that maximizes  $\rho$  determines the angular locations of the targets, as well as their relative RCSs.

To detect multiple targets we apply an adaptive two-step correlation process. First, we correlate the field distribution in the measurement plane with the field distribution due to single target in the measurement database. This would give us an exact angular location of the target if there is only one target, and an approximate location if there are multiple targets. Next, we correlate the measured field

distribution with that due to multiple targets also stored in the database. The advantage of carrying out the first step is that it greatly reduces the number of correlations, once we have determined the approximate location of the targets. This is because we just need to search within the beam-width of the antenna to see if there is a single or multiple targets located within that particular beam-width where the first step detects the presence of single or multiple targets. It is possible to employ some adaptive techniques to further reduce the search complexity. However, the discussion of above issues is beyond the scope of this paper.

To demonstrate the application of the method described, we now consider the above case of one or two targets, though the approach can be extended to detect more than two targets located in close proximity. The CM can achieve a very high resolution if one can accurately locate the maximum correlation coefficient. But, the presence of noise can seriously impair the ability to do so if the number of field sampling points in the measurement plane is small. Thus, not unexpectedly, noise is an important factor that limits the resolution.

We also note that there is a cost involved in terms of higher computational complexity, which arises because we need to compute the correlation for a large number of combinations. For example, if there are two targets within a beam-width and they are randomly located in one of the  $N_1$  possible angles, the possible scales of the amplitudes from the two targets is  $N_2$ , the possible initial phase difference between the scattering waves from the two targets is  $N_3$  then the number of combinations which need to be considered equals  $N_1 \times N_1 \times N_2 \times N_3$ , which can be rather large. However, the computational burden could be reduced by recognizing the fact that each correlation operation is independent and, therefore, the entire process is highly parallelizable. Moreover, the scaling efficiency in parallel or distributed computations would approach unity because the correlation operations with different combinations are totally independent and the communication between the processes is rarely required.

### 3. NUMERICAL RESULTS

The scattered field from a target which is being interrogated by the antenna operating in the receive mode can be treated as a plane wave incident up on the antenna from the direction of the target, and we use a commercial Finite Difference Time Domain (FDTD) [22] code to simulate the antenna geometry, shown in Figure 1, to obtain the field distribution in the measurement plane. We do this for a  $y$ -polarized unit amplitude plane wave for 16 different incident angles, given by  $\varphi = 0^\circ$  and  $\theta$  varying from  $30^\circ$  to  $45^\circ$  with an interval of  $1^\circ$ , and we set the observation frequency to 30 GHz. Figure 3 shows

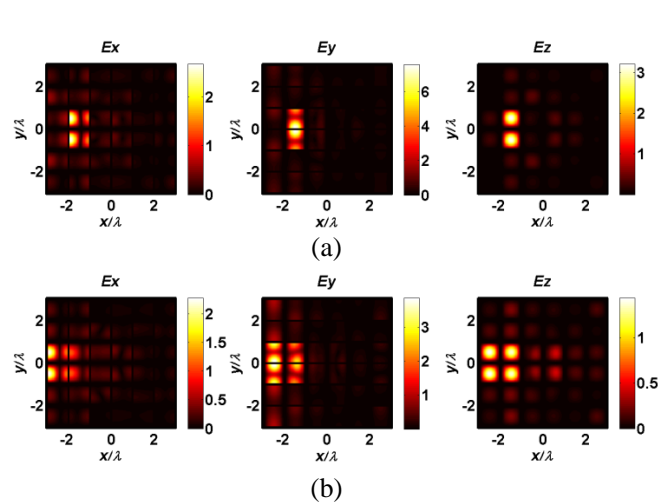


**Figure 3.**  $E_x$ ,  $E_y$  and  $E_z$  field distributions in the measurement plane for different incident angles: (a)  $\theta = 30^\circ$ ; and (b)  $\theta = 40^\circ$ , with  $\varphi = 0^\circ$ .

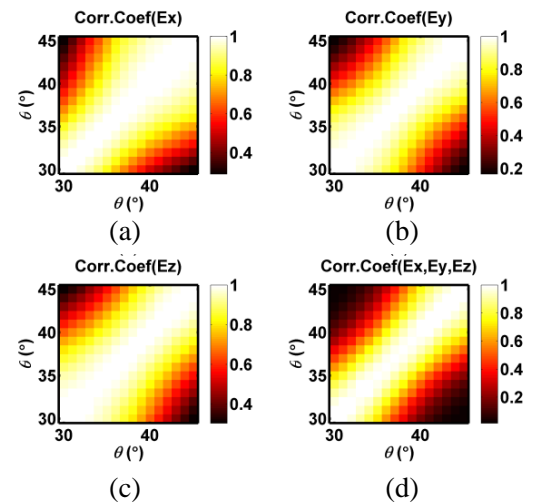


**Figure 4.** Correlation coefficients for (a)  $E_x$ , (b)  $E_y$ , (c)  $E_z$ , and (d) product of the three components, for  $\varphi = 0^\circ$  and  $\theta$  varying from  $30^\circ$  to  $45^\circ$ .

the  $E_x$ ,  $E_y$ ,  $E_z$  field distributions at the measurement plane for a few selected incident angles. We note that  $E_y$  is always higher than  $E_x$  and  $E_z$  because of the incident wave is  $y$ -polarized. Moreover, these field distributions vary slightly with the gradual change in the angle of incidence. The maximum of the field distribution shifts along the negative  $x$ -direction as  $\theta$  varies from  $30^\circ$  to  $45^\circ$ .

The simulated measured field provides us the positions of the samplings at arbitrarily locations in the measurement plane, depending upon the mesh used in the simulation. For plane waves with different incident angles, the meshes used are different and non-uniform. Therefore, we use a linear interpolation algorithm to map the field to uniform grids for the purpose of generating the database that would be used for correlation at a later stage.

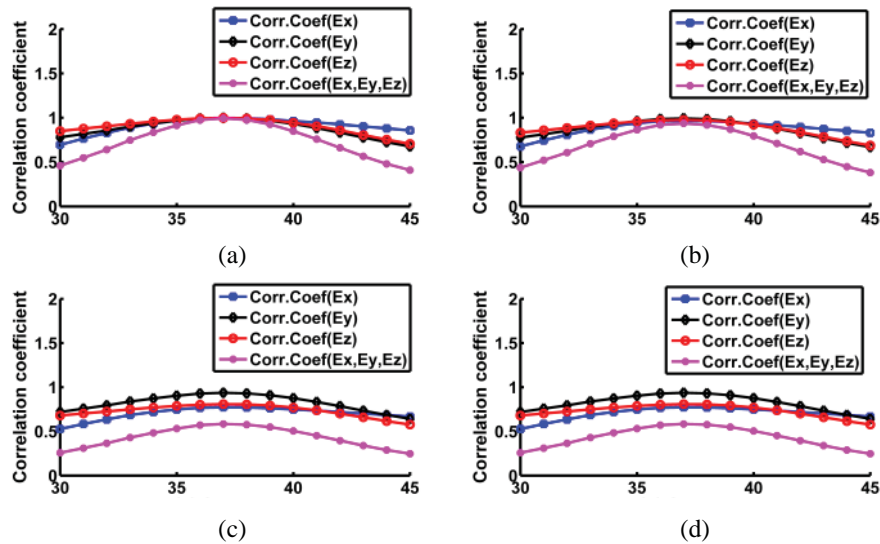
In Figure 4, the correlation coefficients for each individual electric field component, as well as a product of the correlation coefficients of all the three components are presented. The diagonal elements represent the self-correlation coefficients which would be 1 for the ideal case when there is no noise. By comparing Figures 4(a), (b), (c) with (d), it is observed that taking the product of the three correlation coefficients further improves the resolution as compared to the case when just a single electric field component is used. But this comes at the cost of measuring all the three components of the electric field, which requires three separate sensors in a practical implementation.

Figure 5 shows the correlation coefficients for a single target located at an angle of  $\theta = 37^\circ$ ,  $\varphi = 0^\circ$  with different noise levels, e.g., SNR = 35 dB, SNR = 25 dB, SNR = 15 dB, and SNR = 5 dB. Here, we consider the additive Gaussian white noise that has a constant spectral density and a Gaussian distribution of amplitude for convenience. We can find that the correlation coefficients decrease with the increasing of the noise level. It means that the results of the correlation method are affected by noise.

We next investigate the case of two targets with very small angular separation, i.e., less than half-power beam-width. The two angles were randomly chosen from  $30^\circ$  to  $45^\circ$  in  $\theta$  with  $\varphi = 0^\circ$ , and their combined electric field distributions in the measurement plane were derived by using random amplitude scaling factor in the range of  $[0.4, 2.5]$  and random initial phases in the range of  $[0^\circ, 359^\circ]$ . We consider 50 random pairs of incident plane waves. If there is only one target it would correspond to the case when 1st and 2nd angles are the same. The total fields measured in the measurement plane can be expressed as:

$$E_{total} = a_1 e^{j\phi_1} E_1 + a_2 e^{j\phi_2} E_2 = a_1 e^{j\phi_1} \left( E_1 + \frac{a_2}{a_1} e^{j(\phi_2 - \phi_1)} E_2 \right) \quad (3)$$

where  $E_1$  and  $E_2$  are the known electrical fields measured in the measurement plane when uniform



**Figure 5.** Correlation coefficients for a single target located at an angle of  $\theta = 37^\circ$ ,  $\varphi = 0^\circ$ , with: (a) SNR = 35 dB; (b) SNR = 25 dB; (c) SNR = 15 dB; and (d) SNR = 5 dB.

plane waves with unit amplitudes are incident on the lens from two different directions. Also,  $(a_1, \phi_1)$  and  $(a_2, \phi_2)$  are the amplitude scales and initial phases of the fields scattered by the first and second randomly chosen scatterers, respectively.

In the CM, the field distributions in the measurement plane are then correlated with those in the measurement database. The highest value of correlation coefficient estimates the angular location of the targets and their characteristics. In this paper we consider the step of the amplitude scaling factor  $(a_2/a_1)$  as: 1, 1.25, 1.5, 1.75, 2.0, 2.25, 2.5, 1/1.25, 1/1.5, 1/1.75, 1/2.0, 1/2.25 and 1/2.5; we also consider the step of the difference of phase  $(\phi_2-\phi_1)$  as:  $0^\circ, 9^\circ, 18^\circ, \dots, 351^\circ$ . We note that, for a pair of incident angles, with an amplitude step of 0.25 and phase step of  $9^\circ$ , it is necessary to consider a total of  $16 \times 16 \times 10 \times 40$  different combinations that are obtained if we take a combination of 10 cases for the amplitude scaling factor  $(a_2/a_1)$ , and 40 for the initial phase difference  $(\phi_2-\phi_1)$ .

Next, we determine the optimal combination of the amplitude scale step  $(\delta a)$  and the phase difference step  $(\delta \phi)$  to achieve a high resolution. Three different  $\delta a$  and  $\delta \phi$  combinations are considered: (i)  $\delta \phi = 9^\circ$  and  $\delta a = 0.25$ ; (ii)  $\delta \phi = 18^\circ$  and  $\delta a = 0.25$ ; and (iii)  $\delta \phi = 9^\circ$  and  $\delta a = 0.5$ . Figure 6 shows the percentage accuracy for these three cases, computed by using the 50 random pairs of targets in the absence of noise. As expected, the smaller the amplitude scale and phase difference steps, the higher the accuracy we can achieve. In all cases, the angular error in the detection is less than  $2^\circ$ . Also, we note that: (i) results in more accurate estimation at the cost of higher computational complexity. Hence, we choose  $\delta \phi = 9^\circ$  and  $\delta a = 0.25$  to construct the measurement database.

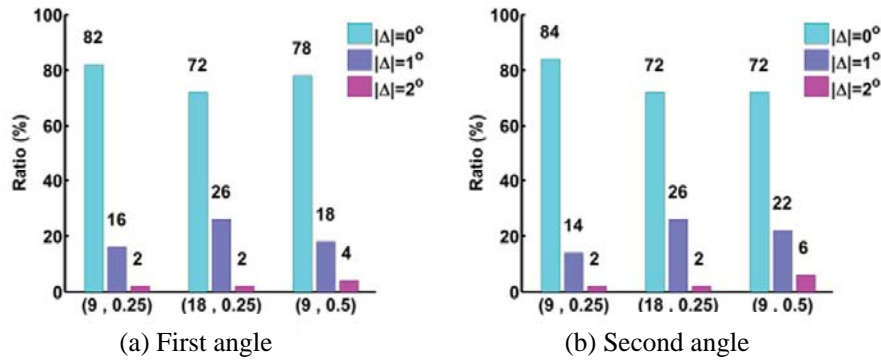


**Figure 6.** Accuracy ratios for (a) first and (b) second incident angle with different search steps: (i)  $\delta \phi = 9^\circ$  and  $\delta a = 0.25$ , (ii)  $\delta \phi = 18^\circ$  and  $\delta a = 0.25$ , and (iii)  $\delta \phi = 9^\circ$  and  $\delta a = 0.5$ .

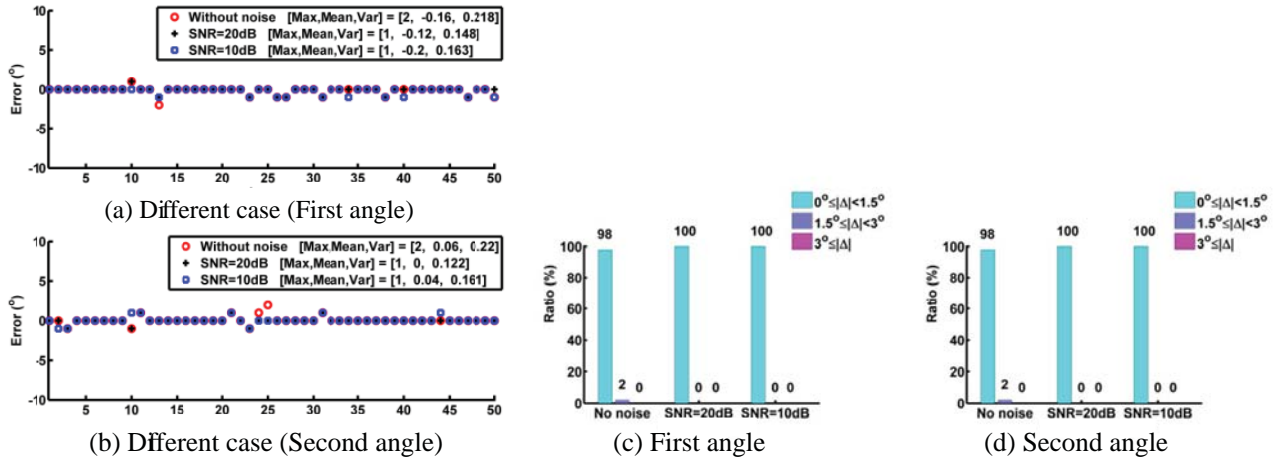


**Figure 7.** Error distributions and accuracy ratios in the estimation results for (a), (c) the first and (b), (d) second incident angle for different SNR with 18 samplings at each waveguide truncation plane.

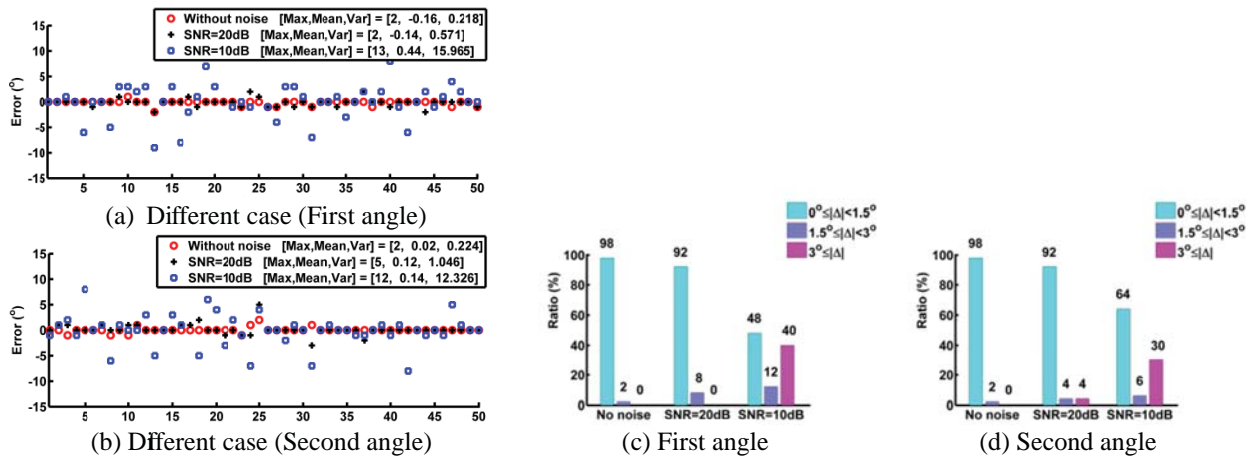


**Figure 8.** Error distributions and accuracy ratios in the estimation results for (a), (c) the first and (b), (d) second incident angle for different SNR with 9 samplings at each waveguide truncation plane.

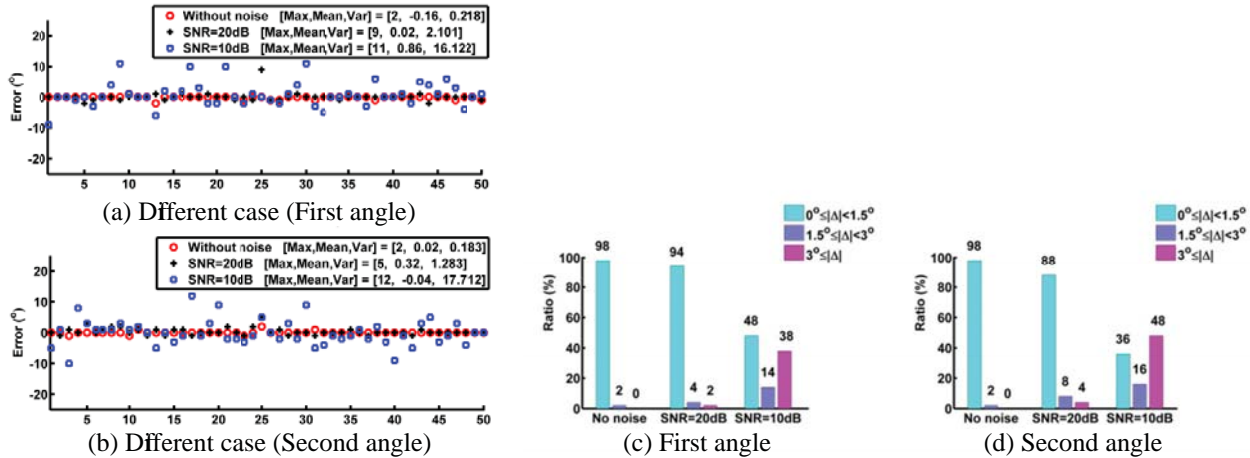


**Figure 9.** Error distributions and accuracy ratios in the estimation results for the (a), (c) first and (b), (d) second incident angle for different SNR with 4 samplings at each waveguide truncation plane.

Figures 7–10 show the target detection error distributions for the 50 random locations of a pair of targets and their percentage target estimation accuracy, for different SNRs and for 18, 9, 4 and 1 field sampling points, respectively, in the  $x$ - and  $y$ -directions for each waveguide in the measurement plane, using search steps of  $\delta\phi = 9^\circ$  and  $\delta a = 0.25$ . It is evident that the target estimation accuracy is more susceptible to noise when the number of field sampling points is lower. However, since it is difficult to measure the fields at a large number of points in a waveguide in practical scenarios, we must resort to a compromise between the target detection accuracy and the number of sampling points. Also, as the SNR decreases to 10 dB, percentage target estimation accuracies achieved are 100%, 50%, 40% and 30%, for 18, 9, 4 and 1 sample, respectively. But, the SNR of a typical radar system can be kept well above 20 dB. Therefore, for a SNR above 20 dB, we are able to achieve percentage target estimation accuracies of 100%, 92%, 91% and 65%, respectively, by using 18, 9, 4 and 1 sample, respectively. The error in the detection in the absence of noise is due to the error introduced by interpolation. Also, it is observed from Figures 7–10 that the maximum error, the mean error and the variance of the error increase as SNR decreases and the number of field sampling point decreases. But these values are within reasonable limits for more than 4 field sampling points in the  $x$ - and  $y$ -directions in the measurement plane for each waveguide with SNR greater than 20 dB.

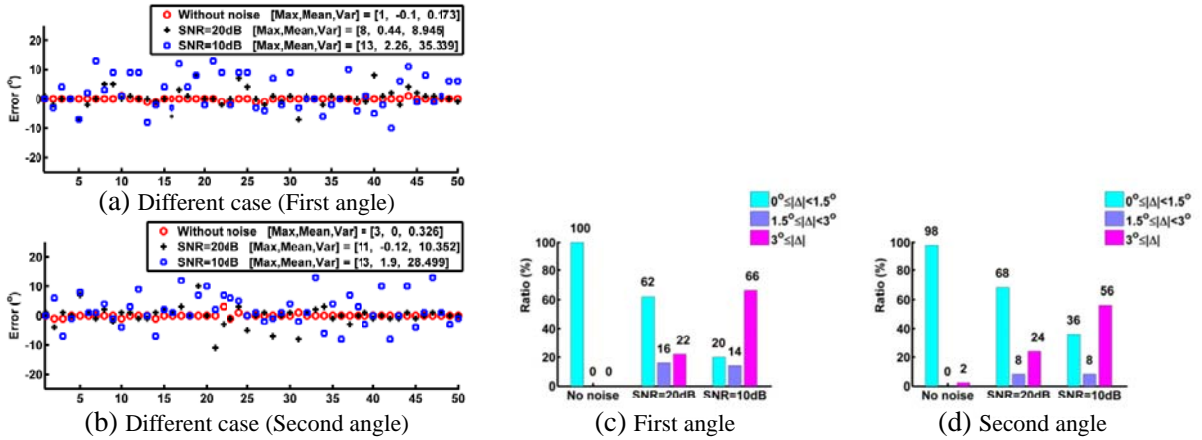


**Figure 10.** Error distributions and accuracy ratios in the estimation results for (a), (c) the first and (b), (d) second incident angle for different SNR with 1 samplings at each waveguide truncation plane.

#### 4. CONCLUSIONS

In this paper, we have presented an adaptive correlation technique to achieve better than half-power beam-width resolution in detecting multiple targets by using the flat-base Luneburg lens antenna. We have shown that it is possible to detect two targets with nearly 90% accuracy for an angular separation as small as  $1^\circ$  and an SNR of 20 dB. Also, it has been shown that the effect of noise could be further reduced by measuring the fields at a larger number of locations on the measurement plane, albeit at an increased computational cost.

#### REFERENCES

- Balanis, C. A., *Modern Antenna Handbook*, Wiley, 2008.
- Lafond, O., M. Himdi, H. Merlet, and P. Lebars, "An active reconfigurable antenna at 60 GHz based on plate inhomogeneous lens and feeders," *IEEE Trans. Antennas Propag.*, Vol. 61, No. 4, 1672–1678, 2013.
- Mirkamali, A., J.-J. Laurin, F. Siaka, and R. Deban, "A planar lens antenna with circular edge inspired by gaussian optics," *IEEE Trans. Antennas Propag.*, Vol. 61, No. 9, 4476–4483, 2013.
- Luneburg, R. K., *Mathematical Theory of Optics*, University of California Press, 1964.
- Demetriadou, A. and Y. Hao, "A grounded slim Luneburg lens antenna based on transformation electromagnetics," *IEEE Antennas and Wireless Propag. Lett.*, Vol. 10, 1590–1593, 2011.
- Mosallaei, H. and Y. Rahmat-Samii, "Nonuniform Luneburg and two-shell lens antennas: Radiation characteristics and design optimization," *IEEE Trans. Antennas Propag.*, Vol. 49, No. 1, 60–69, 2001.
- Pfeiffer, C. and A. Grbic, "A printed, broadband Luneburg lens antenna," *IEEE Trans. Antennas Propag.*, Vol. 58, No. 9, 3055–3059, 2010.
- Bosiljevac, M., M. Casaletti, F. Caminita, Z. Sipus, and S. Maci, "Non-uniform metasurface Luneburg lens antenna design," *IEEE Trans. Antennas Propag.*, Vol. 60, No. 9, 4065–4073, 2012.
- Dockrey, J. A., M. J. Lockyear, S. J. Berry, S. A. R. Horsley, J. R. Sambles, and A. P. Hibbins, "Thin metamaterial Luneburg lens for surface waves," *Physical Review B*, Vol. 87, 125137, 2013.
- Mirkamali, A. and J.-J. Laurin, "Two-dimensional loaded wire grid for modelling dielectric objects and its application in the implementation of Luneburg lenses," *IET Microw. Antennas Propag.*, Vol. 6, No. 15, 1728–1737, 2012.
- Rondineau, S., M. Himdi, and J. Sorieux, "A sliced spherical Luneburg lens," *IEEE Antennas and Wireless Propag. Lett.*, Vol. 2, 163–166, Feb. 2003.

12. Wu, L., X. Tian, M. Yin, D. Li, and Y. Tang, "Three-dimensional liquid flattened Luneburg lens with ultra-wide viewing angle and frequency band," *Appl. Phys. Lett.*, Vol. 103, 084102, 2013.
13. Wu, L., X. Tian, H. Ma, M. Yin, and D. Li, "Broadband flattened Luneburg lens with ultra-wide angle based on a liquid medium," *Appl. Phys. Lett.*, Vol. 102, 074103, 2013.
14. Ma, H. F. and T. J. Cui, "Three-dimensional broadband and broad-angle transformation-optics lens," *Nature Communications*, 2010, Doi: 10.1038/ncomms1126.
15. Dhoubi, A., S. N. Burokur, A. Lustrac, and A. Priou, "Compact metamaterial-based substrate-integrated Luneburg lens antenna," *IEEE Antennas and Wireless Propag. Lett.*, Vol. 11, 1504–1507, 2012.
16. Hua, C., X. Wu, N. Yang, and W. Wu, "Air-filled parallel-plate cylindrical modified Luneburg lens antenna for multiple-beam scanning at millimeter-wave frequencies," *IEEE Trans. Microw. Theory Tech.*, Vol. 61, No. 1, 436–443, 2013.
17. Ma, H. F., B. G. Cai, T. X. Zhang, Y. Yang, W. X. Jiang, and T. J. Cui, "Three-dimensional gradient-index materials and their applications in microwave lens antennas," *IEEE Trans. Antennas Propag.*, Vol. 61, No. 5, 2561–2569, 2013.
18. James, G., A. Parfitt, J. Kot, and P. Hall, "A case for the Luneburg lens as the antenna element for the square-kilometre array radio telescope," *Radio Science Bulletin*, Vol. 293, 32–37, Jun. 2000.
19. Liang, M., X. Yu, S.-G. Rafael, W.-R. Ng, M. E. Gehm, and H. Xin, "Direction of arrival estimation using Luneburg lens," *IEEE International Microwave Symposium (IMS) Digest (MTT)*, 1–3, Jun. 17–22, 2012.
20. Jain, S. and R. Mittra, "Flat-base broadband multibeam Luneburg lens for wide angle scan," *IEEE Antennas and Propagation Society International Symposium (APS)*, Memphis, TN, 2014.
21. Kendall, M. G. and J. D. Gibbons, *Rank Correlation Methods*, Oxford University Press, 1990.
22. Yu, W., X. Yang, Y. Liu, R. Mittra, and A. Muto, *Advanced FDTD Methods: Parallelization, Acceleration, and Engineering Applications*, Artech House, Norwood, MA, USA, Mar. 2011.